



UDC 620.193.2, 621.793

<https://doi.org/10.17073/1997-308X-2024-5-19-29>

Research article

Научная статья



High-entropy coatings in the FeCrNiCo–Mo_x system with enhanced corrosion and tribocorrosion resistance in seawater

K. A. Kuptsov[✉], M. N. Fatykhova, A. N. Sheveyko, R. T. Islamov,
A. A. Zaitsev, D. V. Shtansky

National University of Science and Technology “MISIS”
1 Bld, 4 Leninskiy Prosp., Moscow 119049, Russia

✉ kuptsov.k@gmail.com


Abstract. To tackle the pressing challenge of protecting steel products in marine and coastal infrastructure from corrosion and tribocorrosion, high-entropy coatings in the FeCrNiCo–Mo_x system were developed using automated vacuum electrospark deposition with specialized equipment. Discs with a diameter of 30 mm made from 30Kh13 steel were used as substrates. The coatings were applied using FeCrNiCo–Mo_x electrodes, where $x = 0, 5, 10$, and 15 at. %, produced by powder metallurgy. The structure, elemental, and phase compositions of the coatings were evaluated using XRD, SEM, and EDS methods. FeCrNiCo–Mo_x coatings were obtained through the remelting of the substrate and electrode material. Coatings with a moderate molybdenum content (2–5 at. %) formed a single-phase solid solution with an FCC lattice. At a Mo content of around 7 at. %, the formation of a second phase based on molybdenum with a BCC lattice was observed. The thickness of the FeCrNiCo coatings was 45 μm , while the addition of molybdenum to the coatings reduced this thickness to 32–34 μm . The corrosion and tribocorrosion resistance of the coatings was assessed in artificial seawater using electrochemical and tribological methods. Under stationary corrosion conditions, the coating with 2 at. % Mo exhibited the highest corrosion resistance, with a corrosion potential of 50 mV and a corrosion current density of 2 $\mu\text{A}/\text{cm}^2$. Under tribocorrosion conditions, the coating with 5 at. % molybdenum demonstrated the highest wear resistance, with a value of $2 \cdot 10^{-5} \text{ mm}^3/(\text{N} \cdot \text{m})$.

Keywords: electrospark deposition, vacuum, coatings, seawater, electrochemistry, wear resistance, corrosion resistance, tribocorrosion

Acknowledgments: The research was supported by the Russian Science Foundation, grant No. 20-79-10104-II.

For citation: Kuptsov K.A., Fatykhova M.N., Sheveyko A.N., Islamov R.T., Zaitsev A.A., Shtansky D.V. High-entropy coatings in the FeCrNiCo–Mo_x system with enhanced corrosion and tribocorrosion resistance in seawater. *Powder Metallurgy and Functional Coatings*. 2024;18(5):19–29. <https://doi.org/10.17073/1997-308X-2024-5-19-29>

Высокоэнтропийные покрытия в системе FeCrNiCo–Mo_x с повышенной коррозионной и трибокоррозионной стойкостью в морской воде

К. А. Купцов , М. Н. Фатыхова, А. Н. Шевейко, Р. Т. Исламов,
А. А. Зайцев, Д. В. Штанский

Национальный исследовательский технологический университет «МИСИС»
Россия, 119049, г. Москва, Ленинский пр-т, 4, стр. 1

 kuptsov.k@gmail.com

Аннотация. Для решения актуальной проблемы защиты стальных изделий морской и прибрежной инфраструктуры от коррозии и трибокоррозии были разработаны высокоэнтропийные покрытия в системе FeCrNiCo–Mo_x, получаемые методом автоматизированного электроискрового легирования в вакууме с использованием специальной установки. В качестве подложек применялись диски диаметром 30 мм из стали 30X13. Для нанесения покрытий использовались электроды CrNiCo–xMo, где $x = 0, 5, 10$ и 15 ат. %, полученные методом порошковой металлургии. Структуру, элементный и фазовый составы покрытий оценивали методами РФА, СЭМ и ЭДС. За счет переплава материала подложки и электрода были получены покрытия FeCrNiCo–Mo_x. Покрытия с умеренной долей молибдена (2–5 ат. %) представляют собой однофазный твердый раствор с ГЦК-решеткой. При содержании Mo около 7 ат. % наблюдается формирование второй фазы на основе молибдена с ОЦК-решеткой. Толщина покрытий FeCrNiCo составляла 45 мкм, введение молибдена в состав покрытий приводило к ее снижению до 32–34 мкм. Оценка коррозионной и трибокоррозионной стойкости покрытий осуществлялась в искусственной морской воде электрохимическими и трибохимическими методами. В стационарных коррозионных условиях покрытие с 2 ат. % Mo характеризовалось наибольшей коррозионной стойкостью: коррозионный потенциал составлял 50 мВ, плотность тока коррозии – 2 мкА/см². В трибокоррозионных условиях наибольшей износостойкостью на уровне $2 \cdot 10^{-5}$ мм³/(Н·м) обладало покрытие с 5 ат. % молибдена.

Ключевые слова: электроискровое легирование, вакуум, покрытия, морская вода, электрохимия, износостойкость, коррозионная стойкость, трибокоррозия

Благодарности: Исследование выполнено за счет гранта Российского научного фонда № 20-79-10104-П.

Для цитирования: Купцов К.А., Фатыхова М.Н., Шевейко А.Н., Исламов Р.Т., Зайцев А.А., Штанский Д.В. Высокоэнтропийные покрытия в системе FeCrNiCo–Mo_x с повышенной коррозионной и трибокоррозионной стойкостью в морской воде. *Известия вузов. Порошковая металлургия и функциональные покрытия*. 2024;18(5):19–29.
<https://doi.org/10.17073/1997-308X-2024-5-19-29>

Introduction

Currently, over 50 % of the world's population lives within 60 km of the coastline [1]. More than 80% of global trade is conducted by sea [2; 3]. Human economic activity in the marine and coastal zones is closely linked to the production and operation of marine transport vessels and coastal infrastructure. Steel, due to its high specific strength, wide availability, and favorable economic characteristics, is one of the primary structural materials used for these purposes [4; 5]. However, the challenges of using structural steels in seawater arise not only from corrosion but also from tribocorrosion – a phenomenon that combines mechanical wear and corrosion degradation [6; 7]. Tribocorrosion causes the most damage to friction pairs, such as bearings, shafts, rods, swivels, etc. [8], leading to a significant reduction in the service life of structures and resulting in substantial economic losses. In industria-

lized countries, the economic impact of tribocorrosion can account for up to 3–4 % of GDP [9; 10].

The primary method of corrosion control in marine environments is alloying steel with chromium and molybdenum due to their ability to form a dense passive film on the surface [11–13]. This film acts as a barrier, preventing contact between the metal and the aggressive environment, thereby protecting against further degradation. However, a recently discovered class of high-entropy alloys (HEAs) has outperformed traditional chromium- and molybdenum-enriched stainless steels in terms of tribocorrosion resistance [14–16]. Fe-based HEAs (Fe–Cr–Ni–Co–X) are promising materials for use in the marine industry due to their excellent mechanical and corrosion properties. Chromium promotes the formation of a stable and dense passive film, with high chromium content enhancing resistance to pitting corrosion. Nickel contributes to resistance

against both general and localized corrosion and serves as an austenite stabilizer. Cobalt also plays a role in stabilizing the oxide film. However, the key element ensuring the formation of a dense and high-quality passive film, especially in the presence of chromium, is molybdenum.

The cost of high-entropy alloys is relatively high due to the substantial content of expensive alloying elements and the complex manufacturing process. Additionally, some HEAs have shown a tendency toward brittle behavior under certain conditions [17].

The most promising application of high-entropy alloys for corrosion protection is not in the fabrication of entire structural components from HEAs but in their use as surface coatings. Currently, HEA-based coatings are primarily produced by methods such as laser cladding, electro-spark deposition, magnetron sputtering, and others [18; 19].

Electro-spark deposition (ESD) in a vacuum using CNC-controlled equipment is one of the most promising methods for producing wear-resistant and corrosion-resistant coatings on various steels due to its improved uniformity and purity [20]. This method can produce relatively thick coatings, up to 200 μm [18; 21], with excellent adhesion strength due to micrometallurgical reactions between the electrode and the substrate. Additionally, this coating technology is characterized by its relative simplicity, cost-effectiveness, high productivity, ease of process automation, and the capability for localized coating deposition. During vacuum electro-spark deposition, material transfer from the electrode to the substrate and pulsed cathode-arc evaporation of the electrode, initiated by spark discharge, occur simultaneously. This enhances process efficiency and improves surface wettability, resulting in lower coating roughness [10].

The aim of this study was to investigate the influence of molybdenum on the structure, corrosion, and tribocorrosion properties of coatings based on the FeCrNiCo–Mo_x high-entropy alloy.

Materials and methods

The FeCrNiCo–Mo_x were deposited using a specialized vacuum system for electrospark deposition, equipped with a three-axis table and a rotating electrode holder [22]. the electrodes used for the coatings were produced by powder metallurgy from a base equiatomic mixture of CrNiCo with addition of 5, 10, and 15 at. % Mo. Iron was introduced into the coatings through the mixing of the substrate and electrode material during the electrospark deposition process.

Fig. 1 shows SEM images of high-purity (>99 %) metal powders of Cr (PKh-1S, <63 μm), Ni (PNK-0T2, <20 μm), Co (PK-1u, <1.2 μm), and Mo (PM99.95, <5 μm), which were used to prepare the initial mixture for electrode production. the powders were mixed in a ball mill for 4 h. Blanks were produced from the mixture by cold pressing, followed by sintering in a vacuum furnace at 1300 $^{\circ}\text{C}$ for 60 min (with a residual pressure in the vacuum chamber not exceeding $1 \cdot 10^{-2}$ Pa). After sintering, the electrode blanks were ground to produce rods 60 mm in length and 6 mm in diameter.

Before deposition, the vacuum chamber was evacuated to a pressure of $5 \cdot 10^{-3}$ Pa, after which Ar (99.993 %) was introduced to maintain a working pressure of 20 Pa. the coatings were deposited under the following parameters: electrode rotation speed – 1000 rpm, scanning speed and step – 500 mm/min and 0.5 mm, respectively. After each processing cycle, the scanning direction was changed to perpendicular to ensure better coverage and uniformity of the coatings.

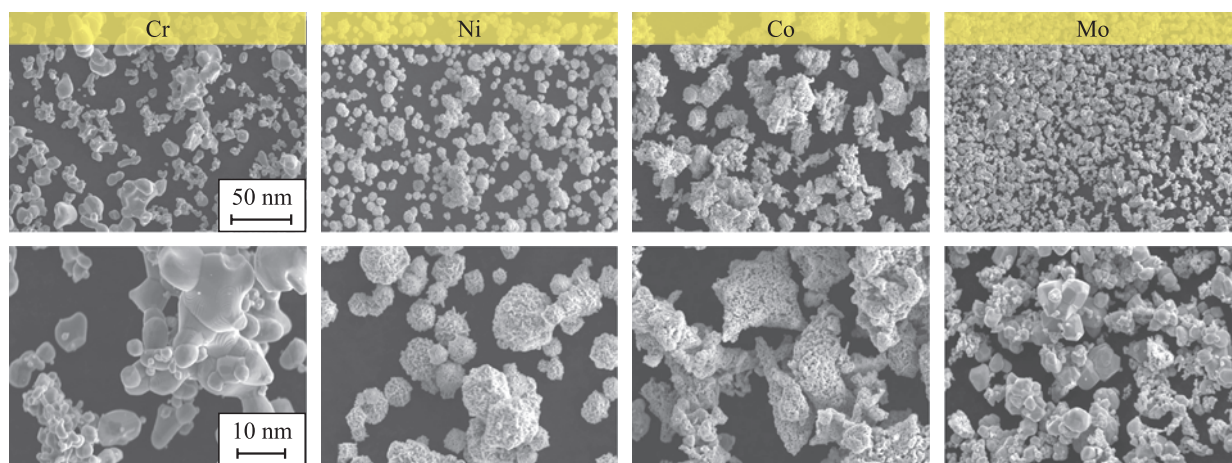


Fig. 1. SEM images of powders used for electrodes production

Рис. 1. СЭМ-изображения порошков, используемых для изготовления электродов

The FeCrNiCo–Mo_x coatings were deposited onto 30 mm diameter, 3 mm thick discs made of 30Kh13 steel under the following technological parameters: pulse frequency – 500 Hz, voltage – 50 V, pulse duration – 50 μs, electrode polarity – anodic.

Phase composition of the coatings was studied using X-ray phase analysis (XRD) on a D8 Advance diffractometer (Bruker, Germany) with monochromatic CuK_α radiation in the 2θ angle range from 10 to 100°.

Morphology and microstructure of the coatings were examined using a scanning electron microscope (SEM) S-3400N (Hitachi, Japan) equipped with an energy-dispersive spectrometer (EDS) NORAN (Thermo Scientific, USA).

Electrochemical properties of the coatings were studied in a three-electrode cell using an IPC Pro MF potentiostat (Russia). A platinum electrode was used as the auxiliary electrode, and an Ag/AgCl electrode served as the reference. the corrosion current density and potential were determined by extrapolating the polarization curves using the Tafel method.

Tribocorrosion resistance of the coatings was evaluated using a Tribometer (CSM Instruments, Switzerland) equipped with a special rotating cell that allows the registration of the electrochemical corrosion potential during tribological tests in a ball-on-disk configuration. the tests were conducted in artificial seawater

at a load of 5 N, a distance of 500 m, and a sliding speed of 10 cm/s. the artificial seawater was prepared according to ASTM D1141-98 from the following salts (g/L): NaCl (24.53), MgCl₂ (5.20), Na₂SO₄ (4.09), CaCl₂ (1.16), KCl (0.695), NaHCO₃ (0.201), KBr (0.1), H₃BO₃ (0.027), SrCl₂ (0.003), NaF (0.003).

An alumina (Al₂O₃) ball with a diameter of 6 mm and a roughness of $R_a = 0.8 \mu\text{m}$ was used as the counterbody. the wear tracks on the coatings were examined using optical profilometry with a WYKO NT1100 profilometer (Veeco, USA).

Results and discussion

Fig. 2 presents SEM cross-sectional images of the electrodes after sintering and the corresponding molybdenum distribution maps. All electrodes were characterized by high density and low residual porosity. Molybdenum in the CoCrNi–5Mo electrode was evenly distributed throughout the volume, while in electrodes with higher Mo content (10 and 15 at. %), clusters rich in molybdenum were observed.

The coatings obtained using the CoCrNi, CoCrNi–5Mo, CoCrNi–10Mo, and CoCrNi–15Mo electrodes are referred to as 0Mo, 5Mo, 10Mo, and 15Mo, respectively. Fig. 3 shows SEM images of the coating surfaces and the corresponding element distribution maps; the composition of the coatings is provided in Table 1.

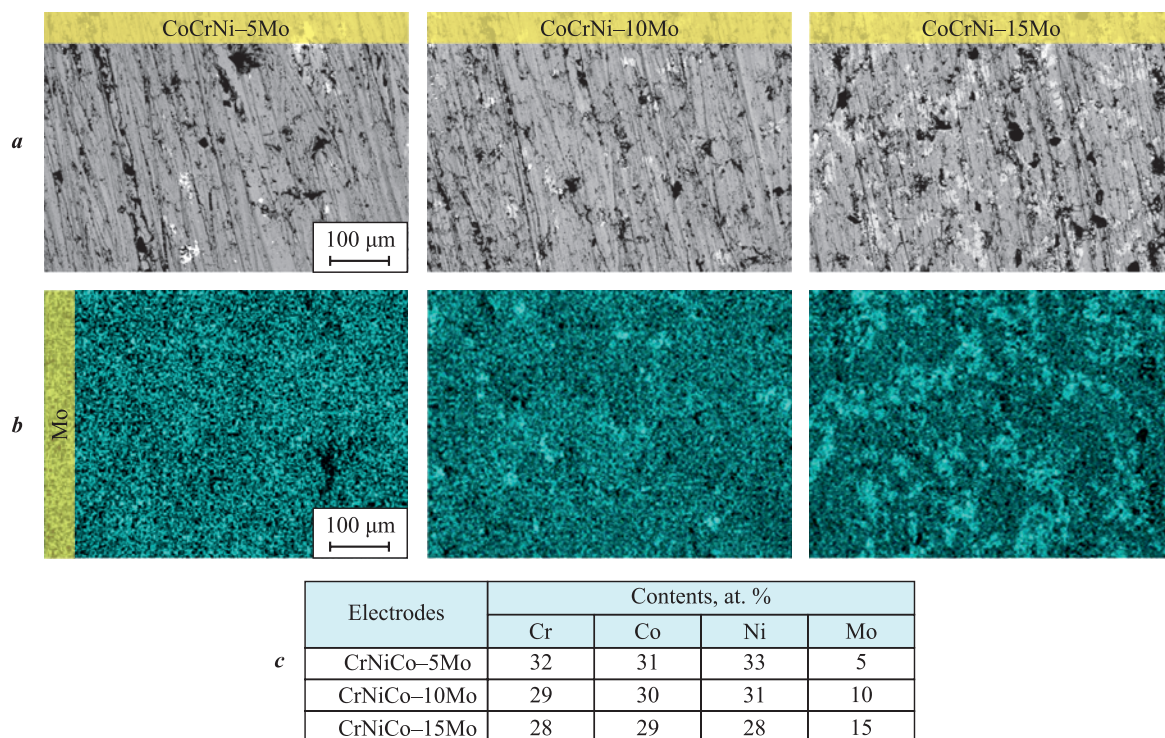


Fig. 2. SEM images of electrode cross-sections (a), Mo distribution maps (b) and elemental composition (c)

Рис. 2. СЭМ-изображения шлифов электродов (a), карты распределения Mo (b) и элементный состав (c)

the surface of the coatings exhibits a characteristic morphology in the form of overlapping areas of solidified melt formed by individual electrospark deposition pulses. No cracks or other surface defects were detected on the coatings. the 0Mo coating was characterized by a uniform distribution of elements across the surface. the introduction of Mo into the coatings resulted in the formation of a less homogeneous structure. It is evident that the 10Mo and 15Mo coatings consist of two distinct areas: 1) iron-based and 2) regions with higher concentrations of Mo, Ni, and Co. Additionally,

Table 1. Elemental composition (at. %) of the surface of FeCrNiCo–Mo_x coatings

Таблица 1. Элементный состав (ат. %) поверхности покрытий FeCrNiCo–Mo_x

Coating	O	Cr	Fe	Co	Ni	Mo
0Mo	4	20	41	16	19	–
5Mo	4	21	41	17	15	2
10Mo	3	24	31	17	20	5
15Mo	5	20	43	12	13	7

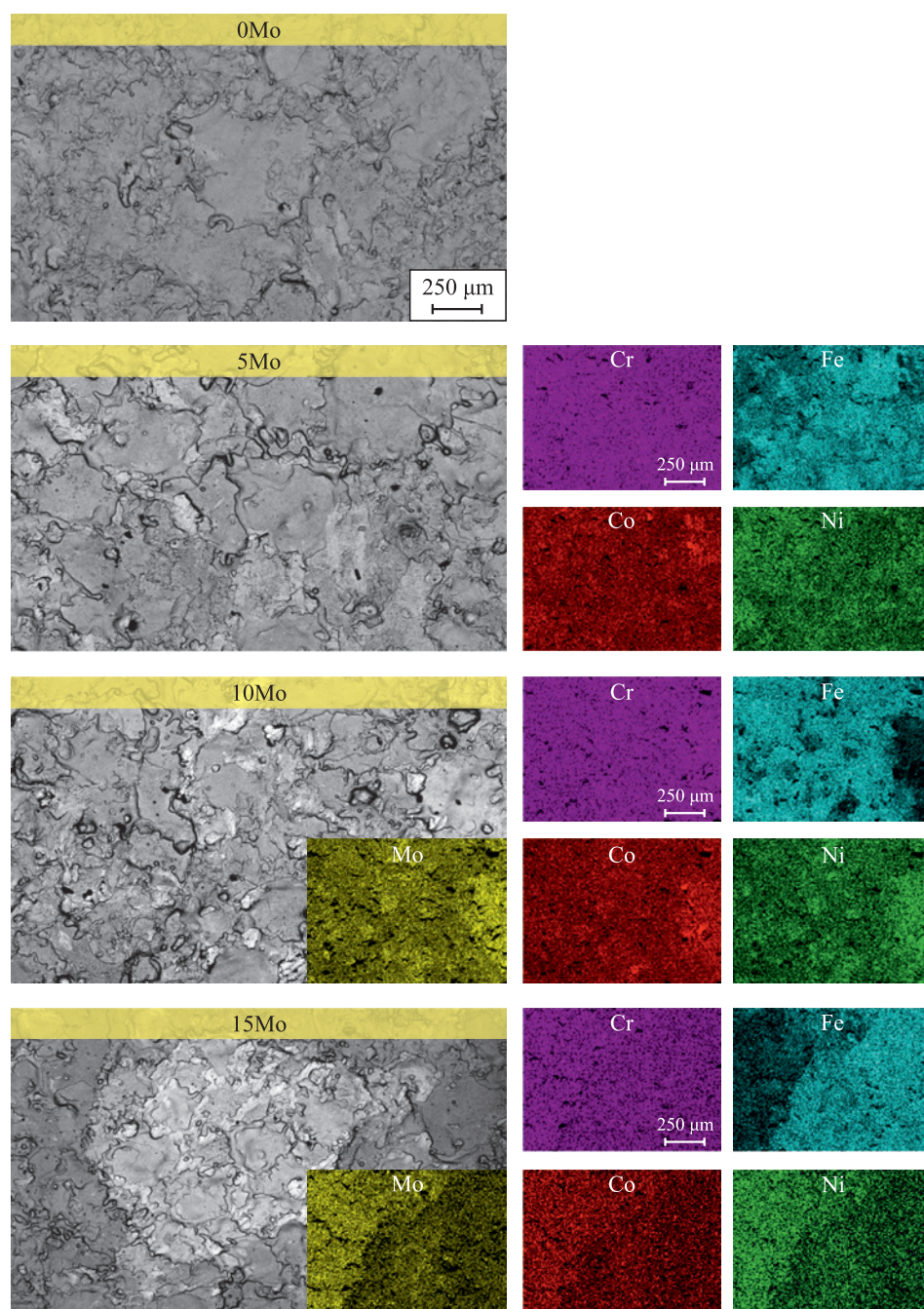


Fig. 3. SEM images of coating surface and corresponding element distribution maps

Рис. 3. СЭМ-изображения поверхности покрытий и соответствующие карты распределения элементов

the coating with the highest molybdenum content exhibited increased surface roughness, with so-called “burns” containing large amounts of molybdenum.

Iron was the primary element in the coatings. the introduction of iron into the coatings occurred directly during electrospark deposition due to the mixing of the melts from both the electrode material and the substrate material in localized melting areas. the 10Mo coating had the lowest iron content, at 31 at. %, while in the other coatings it ranged between 41–43 at. %. This effect is likely due to more intensive transfer of the CoCrNi–10Mo electrode material. the molybdenum content in the coatings increased with its proportion in the electrodes, reaching 2 (5Mo), 5 (10Mo), and 7 (15Mo) at. %, respectively. the 10Mo coating had the highest chromium content of 24 at. %, while the other coatings showed chromium levels in the range of 20–21 at. %. the Ni and Co content in the 0Mo–10Mo coatings was 15–20 at. %, while in the coating with the highest molybdenum content, it was around 12–13 at. %. Additionally, all coatings showed a small oxygen content of about 3–5 at. %.

Fig. 4 shows SEM cross-sectional images of the coatings at various magnifications. the coatings exhibited high density, with no voids or cracks detected. the base FeCrNiCo coating without molybdenum had the highest thickness – up to 45 μm – while processing with molybdenum-containing electrodes reduced the thick-

ness to 32–34 μm (5Mo–15Mo coatings). the reduction in coating thickness is associated with the altered material transfer during processing due to the introduction of refractory molybdenum, which led to a decrease in the size of the melt zone. Additionally, the molybdenum-containing coatings showed more pronounced transition areas between the substrate and the coating. the main layer of the 0Mo and 5Mo coatings was characterized by high uniformity, while the introduction of a higher amount of molybdenum into the coatings resulted in the formation of more distinct areas, rich in molybdenum and depleted in iron (Fig. 4, c). In the 10Mo coatings, these areas appeared as isolated clusters smaller than 5 μm , while in the 15Mo coating, these areas formed a discontinuous top layer.

Fig. 5 presents XRD patterns of FeCrNiCo–Mo_x coatings and the steel substrate. All coatings were characterized by a single-phase structure based on a solid solution with an FCC lattice and a strong (200) texture, formed due to the directional solidification of the melt zones. Increasing the molybdenum content in the coatings leads to a shift of the FCC peaks towards lower angles, indicating an increase in the lattice parameter due to the large atomic radius of molybdenum. It is worth noting that the 10Mo and 15Mo coatings have the same lattice parameter, which may be due to the small difference in molybdenum content (5 and 7 at. %) and the fact that when the molybdenum con-

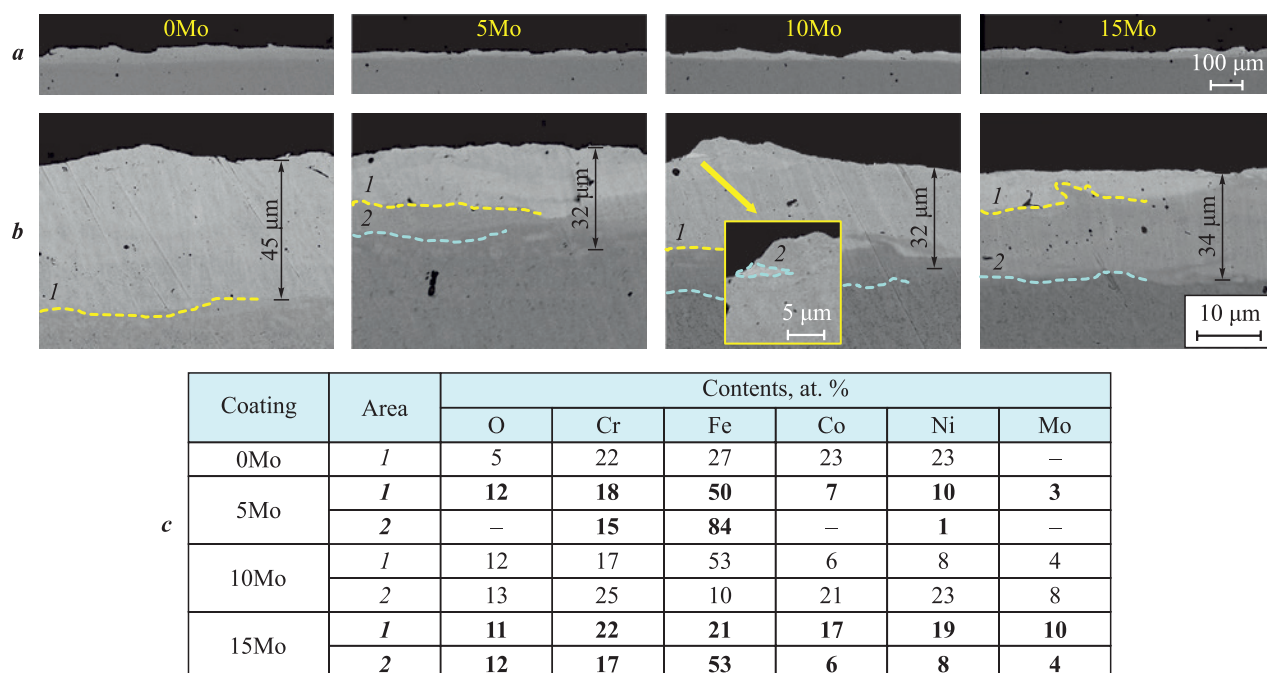


Fig. 4. SEM images of cross-sections of FeCrNiCo–Mo_x coatings at different magnifications (a, b) and elemental composition of selected areas (c)

Рис. 4. СЭМ-изображения шлифов покрытий FeCrNiCo–Mo_x при различных увеличениях (a, b) и элементный состав выделенных областей (c)

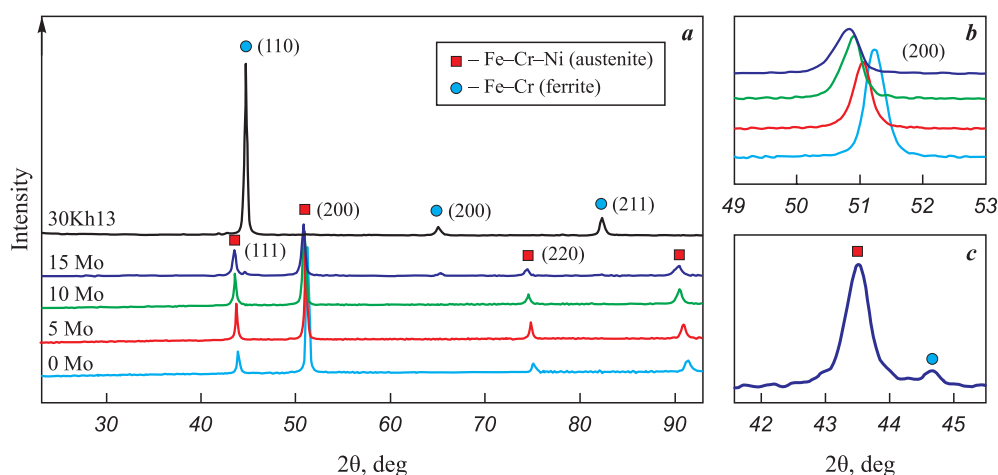


Fig. 5. XRD patterns of FeCrNiCo–Mo_x coatings and 30Kh13 substrate (a), as well as detailed image of FCC (200) peaks (b) and 15Mo coating (111) FCC and (110) BCC phases peaks (c)

Рис. 5. Дифрактограммы покрытий FeCrNiCo–Mo_x и подложки 30X13 (a), а также увеличенное изображение пика (200) ГЦК-фазы (b) и пиков (111) ГЦК- и (110) ОЦК-фаз для покрытия 15Mo (c)

tent exceeds a certain threshold (5 at. % in our case), additional molybdenum can no longer be incorporated into the FCC lattice and will form its own phase.

In the case of the 15Mo coating, a second set of low-intensity peaks corresponding to an α -Fe (ferrite) phase can be distinguished. On one hand, these peaks could be attributed to the substrate, which has this structure. On the other hand, given the thickness of the coatings, this assumption seems unlikely. Another possible explanation is the formation of an additional BCC phase rich in molybdenum. the presence of such regions was shown in the cross-sections of the 15Mo coating. Additionally, molybdenum has very limited solubility in the FCC phase, as it is a ferrite stabilizer. Thus, processing with the CoCrNi–15Mo electrode is undesirable, as it leads to the formation of a two-phase coating.

Fig. 6 presents the results of tribocorrosion tests of FeCrNiCo–Mo_x coatings. These tests included three stages: exposure to a corrosive environment (artificial seawater); tribological testing in a corrosive environment; and re-exposure under stationary conditions after the friction process was completed.

A key characteristic of tribocorrosion is the continuous wear of the passive film, which causes a sharp drop in corrosion potential due to the exposure of an active surface in the corrosive environment. the base 0Mo coating exhibited the highest corrosion potential during friction at –180 mV. Introducing a moderate amount of molybdenum (5Mo and 10Mo coatings) led to a more significant decrease in corrosion potential, down to –200 mV. the coating with the highest Mo content showed the highest drop in corrosion potential to –250 mV, likely due to the formation of galvanic couples between iron- and molybdenum-rich regions.

the coefficient of friction for all coatings ranged from 0.2 to 0.3, with the lowest levels (0.2–0.25) observed in the 0Mo and 10Mo coatings.

The highest wear resistance was observed in the 10Mo and 15Mo coatings with higher molybdenum content – the wear rate was $(2.0 \div 2.7) \cdot 10^{-5} \text{ mm}^3/(\text{N} \cdot \text{m})$, whereas in the 0Mo and 5Mo coatings, it was $(4.1 \div 4.8) \cdot 10^{-5} \text{ mm}^3/(\text{N} \cdot \text{m})$. This effect is likely due to the strengthening of the high-entropy matrix in the 10Mo and 15Mo coatings through the formation of molybdenum-rich regions.

Wear tracks and the composition of wear products are shown in Fig. 7 and Table 2. the morphology of the wear tracks represents partially worn roughness, and the wear products are mainly represented by iron and chromium oxides.

The polarization curves of the coatings with varying Mo content are shown in Fig. 8. the corrosion potential and current density of the base FeCrNiCo coatings were 70 mV and $3.5 \mu\text{A}/\text{cm}^2$, respectively. the introduction of 2 at. % Mo (5Mo coating) led to a slight shift of the potential in the negative direction to 50 mV, but at the same time, the corrosion current density decreased by almost a half ($2 \mu\text{A}/\text{cm}^2$). Further increasing the molybdenum content to 5–7 at. % (10Mo, 15Mo) caused an increase in the electrochemical potential to 110–120 mV; however, the corrosion current density increased to $4.0\text{--}4.5 \mu\text{A}/\text{cm}^2$. Thus, the introduction of a small amount of molybdenum into FeCrNiCo leads to a reduction in corrosion current density, while further increases in molybdenum content primarily result in a significant shift in corrosion potential towards positive values.

This electrochemical behavior can be explained as follows. the introduction of a small amount of molyb-

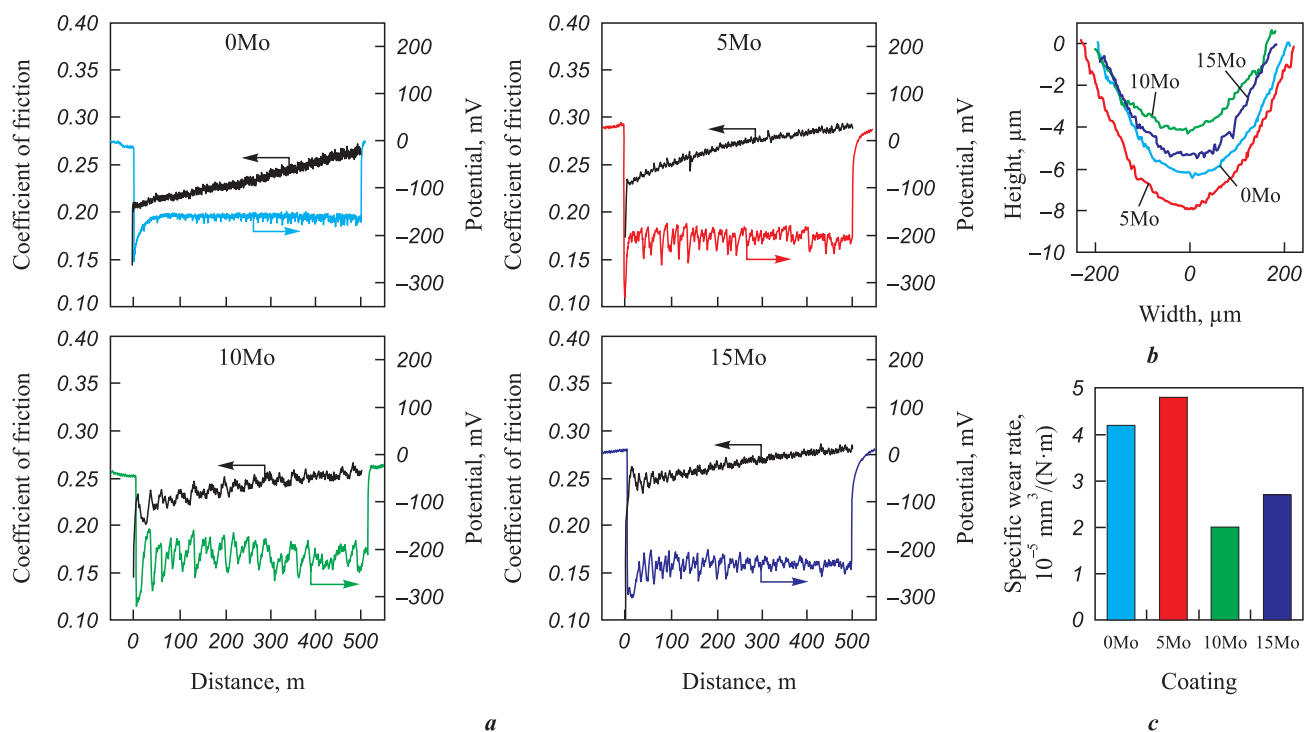


Fig. 6. Results of tribocorrosion tests (corrosion potential and coefficient of friction) of FeCrNiCo–Mo_x coatings in artificial seawater (a), typical 2D wear track profiles (b) and wear rates (c)

Рис. 6. Результаты трибокоррозионных исследований (потенциал коррозии и коэффициент трения) покрытий FeCrNiCo–Mo_x в искусственной морской воде (a), типичные 2D-профили дорожек износа (b) и значения приведенного износа (c)

denum (2 at. %) does not lead to the formation of molybdenum-rich regions, so the surface potential remains almost unchanged. Nevertheless, molybdenum in such quantities, especially when paired with chromium, contributes to the formation of a denser passive film, which improves the corrosion resistance

of the 5Mo coatings. A higher molybdenum content in the coating leads to the formation of regions (possibly phases) rich in molybdenum, which shifts the surface potential in a more positive direction. However, the presence of surface heterogeneities intensifies corrosion processes.

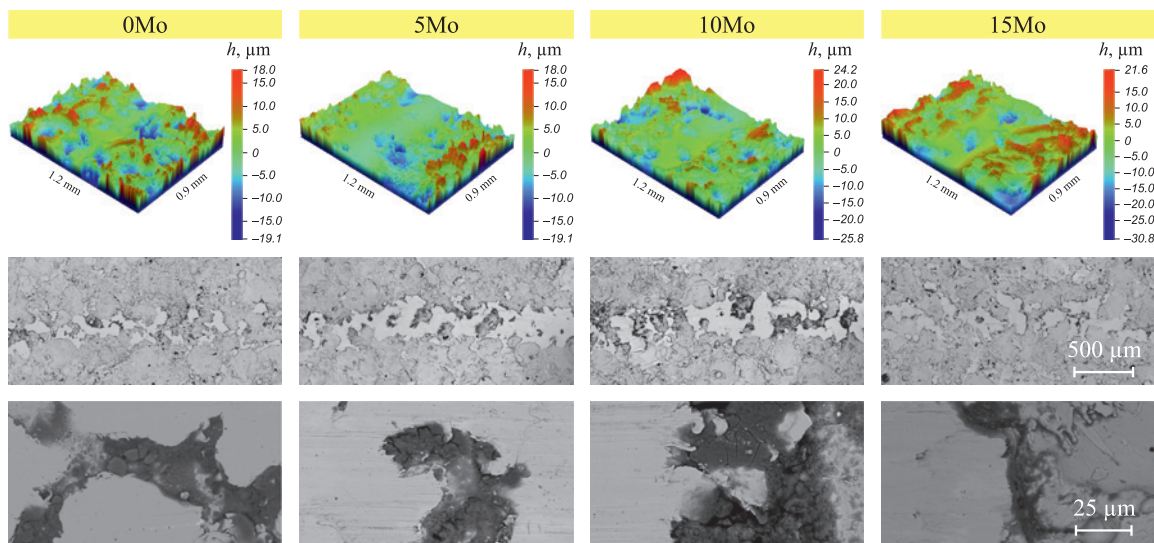


Fig. 7. 3D profiles and SEM images of wear tracks of FeCrNiCo–Mo_x coatings after tribocorrosion tests

Рис. 7. 3D-профили и СЭМ-изображения дорожек износа покрытий FeCrNiCo–Mo_x после трибокоррозионных испытаний

Table 2. Elemental composition of wear products (at. %)

Таблица 2. Элементный состав продуктов износа (ат. %)

Coating	C	O	Na	Mg	Si	Cl	Ca	Cr	Fe	Co	Ni	Mo
0Mo	38	37	1	1	1	1	1	4	10	3	3	–
5Mo	16	58	–	1	1	1	1	4	15	2	1	–
10Mo	18	54	1	1	1	1	1	4	15	2	2	–
15Mo	48	31	1	1	1	1	1	3	10	1	1	1

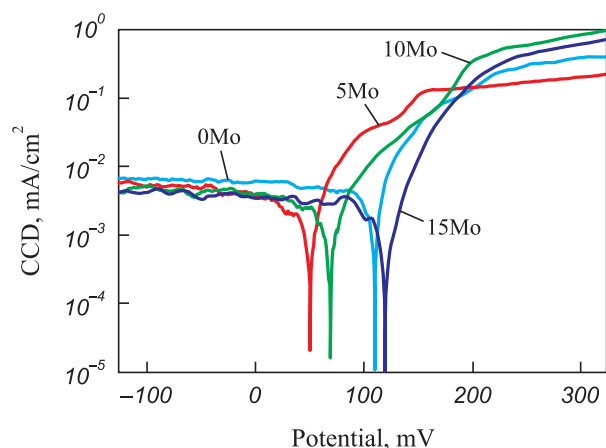


Fig. 8. Corrosion current density versus applied potential curves for coatings with varying molybdenum content

Рис. 8. Зависимости плотности тока коррозии от приложенного потенциала для покрытий с различным содержанием молибдена

Conclusions

1. High-entropy coatings with thicknesses up to 45 μm in the FeCrNiCo–Mo_x system with varying molybdenum content were successfully obtained using electrospray deposition in a vacuum. the introduction of a moderate amount of molybdenum in the range of 2–5 at. % into FeCrNiCo-based coatings has shown promise for enhancing their corrosion and tribocorrosion resistance in seawater.

2. All coatings with molybdenum content up to 5 at. % were single-phase solid solutions with an FCC lattice. the addition of higher amounts of molybdenum (7 at. %) led to the formation of a second phase based on molybdenum with a BCC lattice.

3. Under stationary corrosion conditions, the coating with 2 at. % Mo exhibited the highest corrosion resistance, with a corrosion current density and potential of 2 $\mu\text{A}/\text{cm}^2$ and 50 mV, respectively. the introduction of higher amounts of molybdenum (5–7 at. %) led to a shift in potential towards positive values, up to 120 mV, due to the formation of molybdenum-rich regions. However, the intensified local corrosion caused the corrosion current density to reach 4.5 $\mu\text{A}/\text{cm}^2$.

4. Under tribocorrosion conditions, coatings with moderate molybdenum content (up to 5 at. %) demonstrated a corrosion potential drop to –180 to –200 mV and a coefficient of friction around 0.25. the addition of higher amounts of molybdenum led to a more significant potential drop (down to –250 mV) and a higher coefficient of friction (up to 0.3). the coating with 5 at. % molybdenum exhibited the highest wear resistance, with a specific wear rate of $2 \cdot 10^{-5} \text{ mm}^3/(\text{N} \cdot \text{m})$.

References / Список литературы

- Andres M., Barragan J.M. Development of coastal cities and agglomerations: pressure and impacts on coastal and marine ecosystems. *WIT Transactions on the Built Environment*. 2015;148:63–71. <https://doi.org/10.2495/CC150061>
- Usta O., Korkut E. Prediction of cavitation development and cavitation erosion on hydrofoils and propellers by detached eddy simulation. *Ocean Engineering*. 2019;191: 106512. <https://doi.org/10.1016/j.oceaneng.2019.106512>
- Kruk C.B., Donner M. Freight transport for development toolkit. *Freight Transport for Development Toolkit*. 2009. <https://doi.org/10.1596/27813>
- Abbas M., Rizvi S.H.M., Sarfraz S., Raza A., Khan A., Loya A., Najib A. Evaluation of the influence of dissolved nitrates on corrosion behaviour of ship structural steel exposed to seawater environment. *Ocean Engineering*. 2024;298:117268. <https://doi.org/10.1016/J.OCEANENG.2024.117268>
- Tiamiyu A.A., Eduok U., Odeshi A.G., Szpunar J.A. Effect of prior plastic deformation and deformation rate on the corrosion resistance of AISI 321 austenitic stainless steel. *Materials Science and Engineering*. 2019;745:1–9. <https://doi.org/10.1016/J.MSEA.2018.12.093>
- Liu Z.X., Li Y., Xie X.H., Qin J., Wang Y. the tribo-corrosion behavior of monolayer vn and multilayer VN/C hard coatings under simulated seawater. *Ceramics International*. 2021;47:25655–25663. <https://doi.org/10.1016/J.CERAMINT.2021.05.291>
- Sofiani F.M., Tacq J., Elahi S.A., Chaudhuri S., De Waele W. A hybrid probabilistic-deterministic framework for prediction of characteristic size of corrosion pits in low-carbon steel following long-term seawater exposure. *Corrosion Science*. 2024;232:112039. <https://doi.org/10.1016/J.CORSCI.2024.112039>
- Liu C., Jiang Z., Zhao J., Cheng X., Liu Z., Zhang D. Influence of rare earth metals on mechanisms of localised

- corrosion induced by inclusions in Zr–Ti deoxidised low alloy steel. *Corrosion Science*. 2020;166:108463. <https://doi.org/10.1016/j.corsci.2020.108463>
9. Okoani A.O., Nand A., Ramezani M. Corrosion and wear interplay: Tribo-electrochemical evaluation of NiTiNOL60 alloy in sulfuric acid. *Results in Materials*. 2024;21:100523. <https://doi.org/10.1016/J.RINMA.2023.100523>
 10. Sun Y. Surface engineering & coating technologies for corrosion and tribocorrosion resistance. *Materials*. 2023;16(13):4863. <https://doi.org/10.3390/MA16134863>
 11. Santos R.F., Rocha A.M.F., Bastos A.C., Cardoso J.P., Rodrigues F., Fernandes C.M., Sacramento J., Ferreira M.G.S., Senos A.M.R., Fonseca C. Microstructural characterization and corrosion resistance of WC–Ni–Cr–Mo composite – the effect of Mo. *International Journal of Refractory Metals and Hard Materials*. 2020;86:105090. <https://doi.org/10.1016/J.IJRMHM.2019.105090>
 12. Fu Y., Zhou F., Zhang M., Wang Q., Zhou Z. Structural, mechanical and tribocorrosion performances of CrMoSiN coatings with various Mo contents in artificial seawater. *Applied Surface Science*. 2020;525:146629. <https://doi.org/10.1016/J.APSUSC.2020.146629>
 13. Ren X., Sun W., Tian S., Zhu C., Qin M., Yang Y., Wu W. Tribological and electrochemical behaviors of FeCoNiCrMo_x HEA coatings prepared by internal laser cladding on 316L steel tube. *Materials Characterization*. 2024;211:113906. <https://doi.org/10.1016/J.MATCHAR.2024.113906>
 14. Niu D., Zhang X., Sui X., Shi Z., Lu X., Wang C., Wang Y., Hao J. Tailoring the tribo-corrosion response of (CrNbTiAlV)C_xN_y coatings by controlling carbon content. *Tribology International*. 2023;179:108179. <https://doi.org/10.1016/J.TRIBOINT.2022.108179>
 15. Kafali M., Doleker K.M., Erdogan A., Sunbul S.E., Icin K., Yildiz A., Gok M.S. Wear, corrosion and oxidation characteristics of consolidated and laser remelted high entropy alloys manufactured via powder metallurgy. *Surface and Coatings Technology*. 2023;467:129704. <https://doi.org/10.1016/J.SURFCOAT.2023.129704>
 16. Zeng C., Neils A., Lesko J., Post N. Machine learning accelerated discovery of corrosion-resistant high-entropy alloys. *Computational Materials Science*. 2024;237:112925. <https://doi.org/10.1016/J.COMMATSCI.2024.112925>
 17. Li Q.H., Yue T.M., Guo Z.N., Lin X. Microstructure and corrosion properties of alcoerfeni high entropy alloy coatings deposited on AISI 1045 steel by the electrospark process. *Metallurgical and Materials Transactions A: Physical Metallurgy and Materials Science*. 2013;44:1767–1778. <https://doi.org/10.1007/S11661-012-1535-4/FIGURES/15>
 18. Kuptsov K.A., Antonyuk M.N., Sheveyko A.N., Bondarev A.V., Ignatov S.G., Slukin P.V., Dwivedi P., Fraile A., Polcar T., Shtansky D.V. High-entropy Fe–Cr–Ni–Co–(Cu) coatings produced by vacuum electro-spark deposition for marine and coastal applications. *Surface and Coatings Technology*. 2023;453:129136. <https://doi.org/10.1016/J.SURFCOAT.2022.129136>
 19. Zhang C., Lu X., Zhou H., Wang Y., Sui X., Shi Z.Q., Hao J. Construction of a compact nanocrystal structure for (CrNbTiAlV)N_x high-entropy nitride films to improve the tribo-corrosion performance. *Surface and Coatings Technology*. 2022;429:127921. <https://doi.org/10.1016/J.SURFCOAT.2021.127921>
 20. Kuptsov K.A., Antonyuk M.N., Bondarev A.V., Sheveyko A.N., Shtansky D.V. Electrospark deposition of wear and corrosion resistant Ta(Zr)C–(Fe,Mo,Ni) coatings to protect stainless steel from tribocorrosion in seawater. *Wear*. 2021;486–487:204094. <https://doi.org/10.1016/J.WEAR.2021.204094>
 21. Sheveyko A.N., Kuptsov K.A., Antonyuk M.N., Bazlov A.I., Shtansky D.V. Electro-spark deposition of amorphous Fe-based coatings in vacuum and in argon controlled by surface wettability. *Materials Letters*. 2022;318:132195. <https://doi.org/10.1016/J.MATLET.2022.132195>
 22. Sytchenko A.D., Fatykhova M.N., Kuznetsov V.P., Kuptsov K.A., Petrzhek M.I., Kudryashov A.E., Kiryukhantsev-Korneev Ph.V. TaC-based wear-resistant coatings obtained by magnetron sputtering and electro-spark deposition for wedge gate valve protection. *Powder Metallurgy and Functional Coatings*. 2023;17(3):67–78. <https://doi.org/10.17073/1997-308X-2023-3-67-78>

Сытченко А.Д., Фатыхова М.Н., Кузнецов В.П., Купцов К.А., Петржики М.И., Кудряшов А.Е., Кирюханцев Корнеев Ф.В. Покрытия на основе карбида тантала, полученные методами магнетронного распыления и электроискрового легирования, для повышения износостойкости деталей запорной арматуры. *Известия вузов. Порошковая металлургия и функциональные покрытия*. 2023;17(3):67–78. <https://doi.org/10.17073/1997-308X-2023-3-67-78>

Information about the Authors

Konstantin A. Kuptsov – Cand. Sci. (Eng.), Senior Researcher of the Scientific-Educational Center of SHS of MISIS–ISMAN

ORCID: 0000-0003-2585-0733

E-mail: kuptsov.k@gmail.com

Mariya N. Fatykhova – Cand. Sci. (Eng.), Junior Researcher of the Scientific-Educational Center of SHS of MISIS–ISMAN

ORCID: 0000-0001-6817-5999

E-mail: mariya.antonyuck@ya.ru

Aleksandr N. Sheveyko – Researcher of the Scientific-Educational Center of SHS of MISIS–ISMAN

ORCID: 0000-0003-3704-515X

E-mail: sheveyko@mail.ru

Сведения об авторах

Константин Александрович Купцов – к.т.н., ст. науч. сотрудник Научно-учебного центра (НУЦ) СВС МИСИС–ИСМАН

ORCID: 0000-0003-2585-0733

E-mail: kuptsov.k@gmail.com

Мария Николаевна Фатыхова – к.т.н., мл. науч. сотрудник НУЦ СВС МИСИС–ИСМАН

ORCID: 0000-0001-6817-5999

E-mail: mariya.antonyuck@ya.ru

Александр Николаевич Шеveyко – науч. сотрудник НУЦ СВС МИСИС–ИСМАН

ORCID: 0000-0003-3704-515X

E-mail: sheveyko@mail.ru

Rafael T. Islamov – Research Assistant of the Department of Powder Metallurgy and Functional Coating of National University of Science and Technology “MISIS” (NUST MISIS)

✉ **E-mail:** livinoe@bk.ru

Aleksandr A. Zaitsev – Cand. Sci. (Eng.), Senior Researcher of the Laboratory “*In situ* diagnostics of structural transformations” of the Scientific-Educational Center of SHS of MISIS–ISMAN

ORCID: 0000-0001-6934-9137

✉ **E-mail:** aazaitsev@bk.ru

Dmitriy V. Shtansky – Dr. Sci. (Phys.-Math.), Head of the Research Center “Inorganic Nanomaterials” of NUST MISIS, Chief Researcher of the Scientific-Educational Center of SHS of MISIS–ISMAN

ORCID: 0000-0001-7304-2461

✉ **E-mail:** shtansky@shs.misis.ru

Рафаэль Тагирович Исламов – лаборант-исследователь кафедры порошковой металлургии и функциональных покрытий Национального исследовательского технологического университета «МИСИС» (НИТУ МИСИС)

✉ **E-mail:** livinoe@bk.ru

Александр Анатольевич Зайцев – к.т.н., ст. науч. сотрудник лаборатории «*In situ* диагностика структурных превращений» НУЦ СВС МИСИС–ИСМАН

ORCID: 0000-0001-6934-9137

✉ **E-mail:** aazaitsev@bk.ru

Дмитрий Владимирович Штанский – д.ф.-м.н., заведующий научно-исследовательским центром «Неорганические наноматериалы» НИТУ МИСИС, гл. науч. сотрудник НУЦ СВС МИСИС–ИСМАН

ORCID: 0000-0001-7304-2461

✉ **E-mail:** shtansky@shs.misis.ru

Contribution of the Authors



Вклад авторов

K. A. Kuptsov – defined the research objectives and conceptual framework, applied the coatings, described the results, prepared the manuscript, and formulated the conclusions.

M. N. Fatykhova – defined the research objectives and conceptual framework, conducted microstructural studies, electrochemical and tribocorrosion tests, and prepared the graphical materials.

A. N. Sheveyko – described the electrochemical results.

R. T. Islamov – prepared the literature review.

A. A. Zaitsev – performed the XRD analysis.

D. V. Shtansky – defined the research objectives and conceptual framework.

К. А. Купцов – определение цели работы и концепции исследований, нанесение покрытий, описание результатов, подготовка текста статьи, формулировка выводов.

М. Н. Фатыхова – определение цели работы и концепции исследований, проведение микроструктурных исследований, электрохимических и трибокоррозионных испытаний, подготовка графического материала.

А. Н. Шевейко – описание электрохимических результатов.

Р. Т. Исламов – подготовка литературного обзора.

А. А. Зайцев – проведение рентгенофазового структурного анализа.

Д. В. Штанский – определение цели работы и концепции исследований.

Received 16.04.2024

Revised 06.05.2024

Accepted 13.05.2024

Статья поступила 16.04.2024 г.

Доработана 06.05.2024 г.

Принята к публикации 13.05.2024 г.